

## Feature Review

## Ferroelectricity and Rashba effect in 2D organic–inorganic hybrid perovskites

Kai Leng,<sup>1,\*</sup> Runlai Li,<sup>2</sup> Shu Ping Lau,<sup>1</sup> and Kian Ping Loh <sup>2,\*</sup>

**2D hybrid perovskites with strong spin–orbit coupling (SOC) and structural asymmetry represent a new class of quantum materials that can potentially display coexisting ferroelectricity and Rashba spin splitting. Studies on these systems provide insight into the coupling between strain, spin, and electronic degrees of freedom, as well as symmetry and order parameters in the bulk and at the interfaces. We review design principles for ferroelectric hybrid perovskites with tunable band gaps, Rashba spin-split properties, and multiple polar axes. Different from traditional inorganic semiconductors, the composition and chirality of the organic cation, along with the strength of the coupling between the organic and inorganic components, play key roles in deciding the structural asymmetry that drives ferroelectricity and the spin orbit field.**

**Ferroelectric Rashba perovskites**

One of the longstanding aims in **spintronic devices** (see [Glossary](#)) is to modulate the **spin polarization** using an electric field. **Ferroelectric** Rashba semiconductors have attracted significant interest because of the possibility of giant Rashba spin splitting that can be permanent and electrically switchable, opening the way to a new generation of spintronic devices and non-volatile memory devices [1]. One of the prerequisites for **Rashba effects** (i.e., *k*-dependent spin splitting in the band structure) in bulk materials is the lack of inversion symmetry, which is satisfied by ferroelectrics; that is, materials displaying, below the **Curie temperature ( $T_c$ )**, long-range dipolar order with permanent ferroelectric polarization switchable by an electric field. These classes of materials often possess other ferroic orders such as ferroelasticity as well (i.e., spontaneous strain that is switchable by external stress [2,3]), and if the electric polarization of the material can be influenced by external strains such as uniform heating/cooling, stress, and light, they also possess ‘pyroelectric’, ‘piezoelectric’, and ‘photoferroic’ properties [4–7], which render them attractive for applications in smart electronic devices. Researchers are also searching for multiaxial ferroelectric properties in materials (i.e., multiple polar axis) that allow multilevel control of the electrical states in memory resistor devices, which can be useful for mimicking synaptic plasticity and making neural network devices [8–11]. Besides memory devices, the role of ferroelectricity in photovoltaic applications has attracted much attention [12–15]. The anomalously high photovoltage in ferroelectric materials has the potential to exceed the theoretical Shockley–Queisser limit in solar cell devices.

Prototypical ferroelectric materials include perovskite oxides such as BaTiO<sub>3</sub> and PbTiO<sub>3</sub>, but they are brittle and fabrication is costly. Recently, there are increasing interests in organic–inorganic hybrid perovskite ferroelectric materials because of their tunable chemical composition and low-cost solution-phase synthesis [16,17]. Ferroelectricity in lead halide organic–inorganic hybrid perovskites was first explored in CH<sub>3</sub>NH<sub>3</sub>PbX<sub>3</sub> (MAPbX<sub>3</sub>; X is a halide). However, the verification of ferroelectricity in bulk 3D perovskites is shrouded in controversy as they are mostly **centrosymmetric crystals** [18,19]. By contrast, the presence of organic and inorganic moieties in 2D hybrid perovskites allows spontaneous polarization to be coupled to the order and disorder transition of the organic cations, leading to clear signatures of ferroelectricity [20–22].

**Highlights**

2D hybrid organic–inorganic perovskites provide an interesting material platform to investigate the interaction of spin–orbit coupling with different ordered parameters such as ferroelectricity, lattice, topology, and symmetry.

The flexibility in tuning either the organic or the inorganic components in hybrid perovskites allows a rational way to engineer ferroelectricity in 2D hybrid perovskites. Ferroelectric hybrid perovskites are Rashba ferroelectric semiconductors.

Rashba ferroelectric semiconductors are interesting because of the prospects of electrically switchable spin polarization as well as persistent spin helix. The ability to control electron spin by optimizing the Rashba effect can bring new functionality to electronic devices.

<sup>1</sup>Department of Applied Physics, The Hong Kong Polytechnic University, Hung Hom, Kowloon, Hong Kong  
<sup>2</sup>Department of Chemistry, National University of Singapore, Singapore, Singapore

\*Correspondence: [kathy-kai.leng@polyu.edu.hk](mailto:kathy-kai.leng@polyu.edu.hk) (K. Leng) and [chmlhkp@nus.edu.sg](mailto:chmlhkp@nus.edu.sg) (K.P. Loh).

Ruddlesden–Popper perovskites (RPPs) with a general formula  $(\text{RNH}_3)_2(\text{MA})_{n-1}\text{Pb}_n\text{X}_{3n+1}$ , where R is an alkyl or aromatic group and  $n$  is the number of inorganic metal halide perovskite layers, is a popular class of 2D hybrid perovskites for testing the structure and ferroelectric property correlations [23,24]. Besides corner-sharing  $[\text{BX}_6]^{4-}$  octahedra, large aliphatic or aromatic organic cations [e.g.,  $n$ -butylammonium ( $n$ -BA), phenylethylammonium (PEA)] act as spacers to dissect the framework into well-defined 2D slabs [25–27]. The energy of the bands located in the organic and inorganic parts can be tuned independently, thus imparting great flexibility in tuning the electronic properties. In addition, the weak van der Waals interactions among the 2D slabs allow a single quantum-well unit to be prepared by mechanical exfoliation [28,29] or interfacial assembly [30]. The properties of such ultrathin layers are readily modified by strain and substrate effects, providing extra levels of control in tuning interfacial symmetry and excitonic properties.

Organic–inorganic hybrid 2D perovskites that are ferroelectric are also bulk non-centrosymmetric; thus, they are ferroelectric Rashba semiconductors. The presence of heavy elements such as lead and iodine introduces strong **Spin–orbit coupling (SOC)** in the electronic structure. The spin–orbit interaction couples spin degrees of freedom with electronic orbits, thereby providing a link between the spin space and the crystalline lattice. For non-centrosymmetric crystals or at the interface of a centrosymmetric crystal, a **Dresselhaus–Rashba-type SOC** may occur to lift the electron spin degeneracy even in the absence of a magnetic field, leading to the splitting of the valence and/or conduction band edges to result in an indirect band gap [31–34]. Recombination of carriers is slowed by the band-edge shift in  $k$ -space, thus suppressing photoluminescence (PL) and prolonging the lifetime of carriers and their diffusion length [35,36]. In ferroelectric Rashba materials, the Rashba induced spin precession can be controlled by its ferroelectric state. Controlling spin polarization through ferroelectric polarization switching opens novel device paradigms in **2D valleytronics** by incorporating the ferroic order parameters [33,37]. The nonvolatile polarization state in ferroelectric perovskites can influence the Rashba splitting and Rashba **spin orbit field**. More research is needed to understand how the polar direction is coupled to the Rashba spin orbit field. Ferroelectric Rashba perovskite materials can be potentially used as spin sources due to their Rashba spin polarization. If a charge current flows in spin-polarized surface states, it generates a spin accumulation by the **Edelstein effect**, and a 2D charge-to-spin conversion mechanism occurs as a result. In addition, the dielectric segregated structure allows it to serve as tunneling barrier for charge injection.

Methyl ammonium lead iodide perovskites ( $\text{MAPbI}_3$ , where MA = methyl ammonium, Pb = lead) belong to the centrosymmetric space group with  $D_{2h}$  point symmetry; thus, no bulk Rashba effect is expected. However, a dynamic Rashba effect in  $\text{MAPbI}_3$  was reported to occur due to the ultrafast relaxation of  $\text{MA}^+$  that breaks local structural inversion symmetry at the picosecond time-scale [38,39]. Static Rashba effects in  $\text{MAPbBr}_3$  have also been reported to originate from surface reconstruction associated with the  $\text{MA}^+$  cation reorientations [40]. In the case of 2D perovskites, the ordering of the long organic cation can induce inversion symmetry breaking and induces Rashba splitting to occur in the plane perpendicular to the organic barrier. The Rashba splitting energy of  $40 \pm 5$  meV in 2D hybrid perovskite  $(\text{C}_6\text{H}_5\text{C}_2\text{H}_4\text{NH}_3)_2\text{PbI}_4$  is much larger than that in the 3D counterparts [41].

In this review, we discuss the idea of hybrid perovskite semiconductors as a novel class of ferroelectric Rashba materials with electrically switchable **spin texture**. We compare the properties with those of their 3D counterparts (e.g.,  $\text{MAPbX}_3$ ) to highlight the point that 2D hybrid perovskites have stronger Rashba and ferroelectric effects owing to their unique structure. Related to this, we also discuss the mechanism responsible for ferroelectricity in 2D hybrid perovskite materials, as well as the various device configurations that allow us to probe spin-polarization behavior.

## Glossary

**2D valleytronics:** in addition to charge and spin, electrons in a crystalline solid have a valley degree of freedom that determines the electron's position in the crystal momentum space. 2D valleytronics is motivated by a graphene-like band structure comprising two degenerate valleys at  $+K$  and  $-K$ , which is accessible optically, electrically, and magnetically. Valleytronics seeks to use the electron's valley degree of freedom to encode and process information.

**Centrosymmetric crystals:** a centrosymmetric crystal contains an inversion center as one of its symmetry elements. For every point  $(x, y, z)$  in the unit cell there is an indistinguishable point  $(-x, -y, -z)$ .

**Circular photogalvanic effect:** circularly polarized light creates nonequilibrium spin polarization among the two Rashba-split bands. Through the inverse Rashba–Edelstein effect, a circular photogalvanic photocurrent can be generated, and this photocurrent is sensitive to the polarization status of the light.

**Curie temperature ( $T_c$ ):** a ferroelectric crystal demonstrates ferroelectricity only below a certain phase transition temperature, called the  $T_c$ , and are paraelectric above this temperature.

**Datta–Das transistor:** a spin transistor in which the spin current can be modulated by spin–orbit interactions. Sources and drains must be matched in spin polarization to obtain a high 'on' current.

**Dion–Jacobson (D–J) 2D hybrid perovskites:** D–J 2D perovskites adopt the general formulas  $\text{A}'_2\text{B}_{n-1}\text{Pb}_n\text{I}_{3n+1}$  and  $\text{A}''\text{B}_{n-1}\text{Pb}_n\text{I}_{3n+1}$ , respectively. Here,  $\text{A}'$  and  $\text{A}''$  are monovalent and divalent organic cations, respectively; B is a monovalent cation.

**Dresselhaus–Rashba-type SOC:** Dresselhaus SOC is present in crystals lacking bulk inversion symmetry, whereas Rashba SOC arises from the spatial inhomogeneity of an interface or surface. In both cases, SOC causes energy bands to split. In many materials, these two kinds of SOC couple together, resulting in an anisotropy of spin splitting.

**Dyakonov–Perel relaxation mechanism:** spin relaxation in system with broken inversion symmetry.

**Edelstein effect:** a spintronics-related effect in which a charge current is converted into a spin accumulation.

## Molecular mechanism of ferroelectricity and design strategies

### Ferroelectric mechanisms

A ferroelectric compound exhibits a phase transition in the vicinity of  $T_c$ , which involves a structural transition from a high-temperature, high-symmetry paraelectric phase to a low-temperature, low-symmetry ferroelectric phase. Investigation of structural changes leading to the loss of centrosymmetry at  $T_c$  is essential to understand the origin of ferroelectricity. For example, the correlation between the structural parameters can be analyzed to determine how much each building block contributes to the transition temperature; this can be due to: (i) the hydrogen-bond distance; (ii) the distortion or off-center alignment of the metal in the octahedron; and/or (iii) the packing of molecules with permanent dipoles along a polarization axis.

In general, three types of phase-transition mechanisms, or combinations thereof, create spontaneous polarization, and they can be classified as order–disorder type (I), displacive type (II), and mixed order–disorder and displacive type (III). The distinction between I and II depends on whether the paraelectric phase is microscopically nonpolar (displacive) or nonpolar only in a macroscopically or thermally averaged sense (order–disorder). In III, dipolar molecule or ion displacement and hydrogen bonds work synergistically to induce ferroelectricity. The ferroelectric mechanism in organic–inorganic hybrid 2D perovskites could be generalized as III.

The type I mechanism is classically exemplified by  $\text{NaNO}_2$  illustrated in Figure 1A, where the order-to-disorder motion of dipolar  $\text{NO}_2^-$  ion generate ferroelectricity and the Na atom does not have an expressed role in this transition (Figure 1A). However, this simple picture was challenged in 2002 by Ichikawa; by analyzing the thermal behavior of the Na atom from the displacement parameters as well as the separation between the disordered sites, he concluded that the ferroelectric phase transition in  $\text{NaNO}_2$  is not of a pure order–disorder type, but involves ionic displacement [42]. This underscores the difficulty of categorizing these transitions purely as one type or another, because they often involve coupled mechanisms [43].

The displacive type II mechanism can be A-site-driven or B-site-driven ferroelectricity. In  $\text{BaTiO}_3$  ( $\text{ABO}_3$ ), the spontaneous polarization arises from  $\text{Ti}^{4+}$  (B site ion) displacement in the oxygen octahedron (Figure 1B). An example of A site ion displacement is the recently reported all-organic perovskites MDABCO- $\text{NH}_4\text{-I}_3$  (MDABCO = *N*-methyl-*N'*-diazabicyclo[2.2.2]octonium) that have a saturation polarization ( $P_s$ ) ( $22 \mu\text{C}/\text{cm}^2$ ) close to that of the well-known inorganic

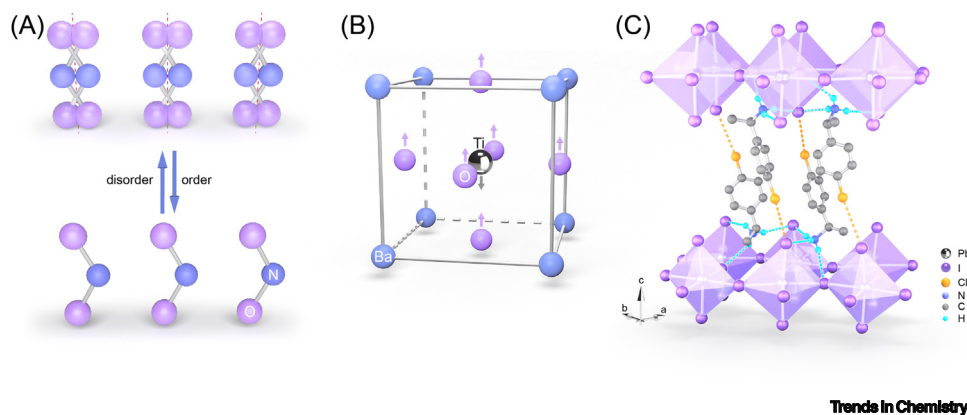


**Figure 1. Three ferroelectric mechanisms.** (A) Order–disorder type. (B) Displacive type. (C) Mixed order–disorder and displacive type. (A,B) Adapted, with permission, from [45]; (C) adapted, with permission, from [49].

**Ferroelectric:** a material lacking an inversion symmetry can develop a spontaneous electric polarization that can be reversed by the application of an external electric field.

**Inverse Edelstein effect:** A non-equilibrium spin accumulation in the plane of a two-dimensional (interfacial) electron gas drives an electric current perpendicular to its own direction, resulting in a 2D spin-to-charge conversion.

**Order–disorder transition:** temperature-dependent collective orientation of organic and inorganic components in a cohesive manner. The order–disorder transition causes structural symmetry changes and accompanies a ferroelectric–paraelectric transition in some cases.

**Persistent spin helix:** a special spin polarization pattern in the momentum space in which the spin is protected from decoherence in a diffusive transport regime, ensuring a long spin lifetime.

**Rashba effects:** Rashba effects or Rashba SOC are usually caused by structure-inversion asymmetry, which stems from the inversion asymmetry of the confining potential (i.e., surface and interfaces). The spin degeneracy of electronic energy bands is lifted by Rashba SOC. Rashba effects provide a mechanism for the generation and manipulation of spins solely through electric fields.

**Spin–orbit coupling (SOC):** a relativistic interaction of a particle's spin with its motion inside a potential. The potential can be due to that of a nucleus or a band structure in a solid. SOC increases with the atomic number  $Z$ ; thus, Pb-based perovskites have strong SOC. SOC can have a Rashba or Dresselhaus contribution.

**Spin orbit field:** in the reference frame of a moving electron, electric fields transform into magnetic fields, which interact with the electron spin and lift the degeneracy of the spin-up and spin-down state.

**Spin polarization:** spin polarization or spin splitting of energy-band states gives rise to magnetic moments in an itinerant model of electronic structure.

**Spin texture:** specific spin configurations in the momentum space induced by the spin orbit field.

**Spintronic device:** performs calculations and stores information using the spin degree of freedom of electrons, envisioned to eventually replace conventional electronics. It also provides

BaTiO<sub>3</sub> [44]. The polarization states are electrically switched by ionic displacement of the A site cation MDABCO. The ferroelectricity in both cases is driven by long-range coulombic interactions.

The ferroelectricity of hybrid organic–inorganic perovskites belongs to the type III mechanism, where the spontaneous polarization is caused by the ordering of the long organic cations and this is coupled to the deformation of the inorganic framework by hydrogen bonds. This is distinct from organic small-molecule ferroelectrics where proton transfer is responsible for the ferroelectricity [45–48]. Figure 1C shows 2D hybrid perovskite with the formula 1-(4-chlorophenyl)ethylammonium]<sub>2</sub>PbI<sub>4</sub> (Figure 1C), in which the organic cation forms a network with the inorganic anion cage using both N–H⋯I hydrogen bonds and C–Cl⋯I–Pb halogen bonds. Increasing the electronegativity of the halogen increases the strength of the hydrogen bond. The **order–disorder transition** of the [R-1-(4-chlorophenyl)ethylammonium] organic cation is coupled to the asymmetry–symmetry transition of the PbI<sub>4</sub><sup>2–</sup> anion via hydrogen bonds; their concerted displacement in opposite directions along the common polar axis (the c-axis) results in in-plane polarization [49]. In addition, strong intermolecular hydrogen bonds impact exciton–phonon coupling in the distorted 2D perovskite lattice, leading to the formation of self-trapped excitons in the distorted lattice and white-light emission [50–52].

#### Origin of ferroelectricity in 2D hybrid perovskites

Ferroelectricity in 2D hybrid perovskites is typically driven by dynamic organic cations. Although the octahedral coordination environment of the inorganic anionic cage has an instability due to symmetry-lowering distortions, that alone does not lead to ferroelectricity unless the motion is coherently coupled to the organic cation [53,54]. The ordering and disordering of the long organic cation drives the paraelectric-to-ferroelectric phase transition. The coherent movement of organic cations and inorganic metal cations (Pb<sup>2+</sup>, Cs<sup>+</sup>) separate the positive and negative charges in opposite directions along a common polar axis and the ‘momentum matching’ of these ions slows molecular rotation during the phase transition [55]. In addition, halogen substitution in the organic cations can induce asymmetry and increases the strength of the hydrogen bonding, increasing the off-centering displacement of ions.

#### Order–disorder of organic cations

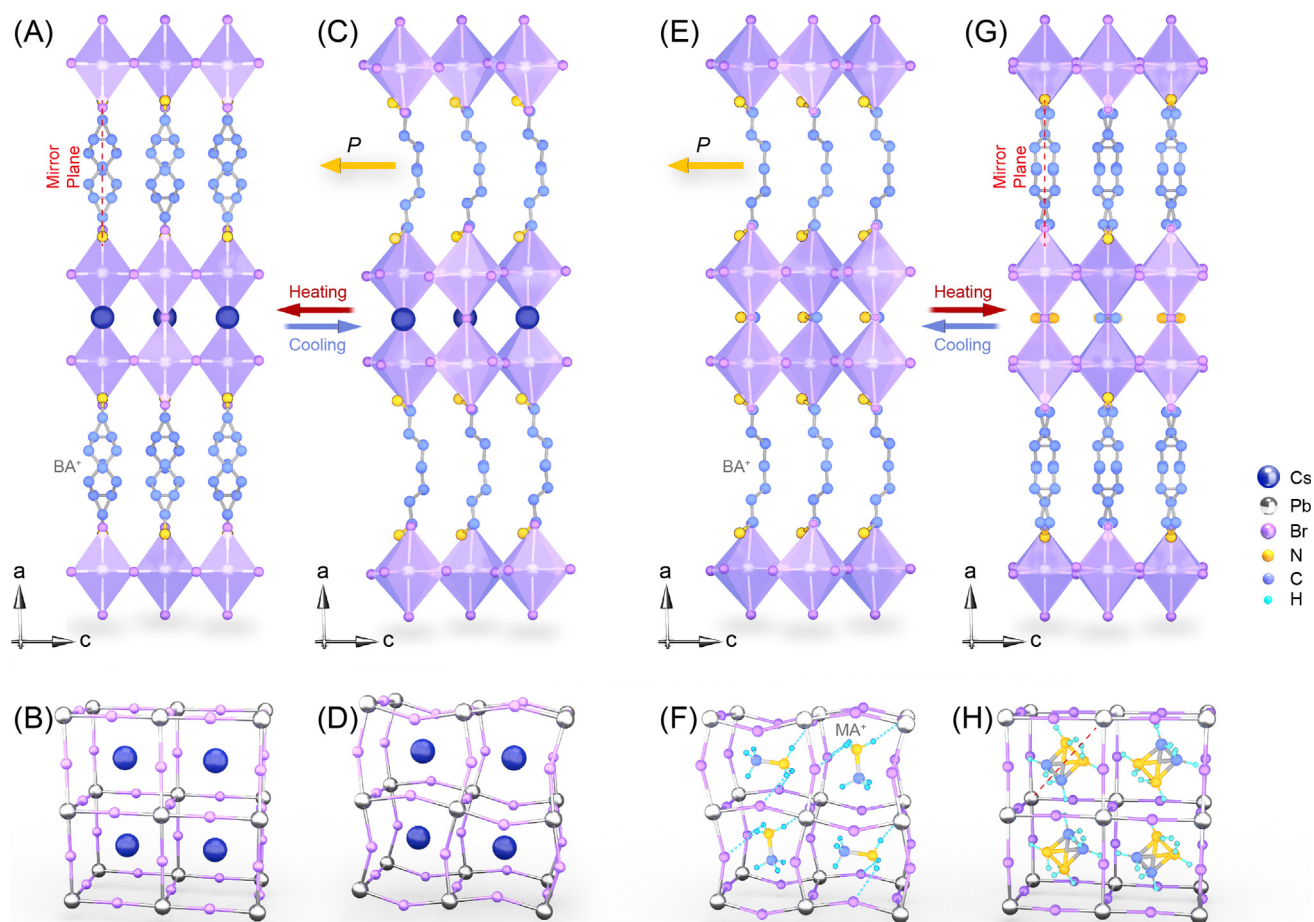
As the paraelectric–ferroelectric phase transition involves a structural phase transition, a detailed structure analysis is indispensable to understand the origin of ferroelectricity. Ferroelectric crystals have to adopt space groups belonging to the ten polar point groups: 1 (*C*<sub>1</sub>), 2 (*C*<sub>2</sub>), *m* (*C*<sub>s</sub>), *mm*2 (*C*<sub>2v</sub>), 3 (*C*<sub>3</sub>), *3m* (*C*<sub>3v</sub>), 4 (*C*<sub>4</sub>), *4mm* (*C*<sub>4v</sub>), 6 (*C*<sub>6</sub>), and *6mm* (*C*<sub>6v</sub>) [43]. Here, typical organic chains in hybrid 2D perovskites were selected to demonstrate structure-related ferroelectricity.

#### Linear alkyl chains

In RPPs, *n*-BA is one of the most typical organic cations selected to form 2D perovskites with lead halides. Ferroelectricity has been reported for hybrid organic–inorganic perovskites of *n*-BA with lead bromides and lead chloride. *P*<sub>s</sub> values of 2.1 μC/cm<sup>2</sup>, 4.2 μC/cm<sup>2</sup>, 3.6 μC/cm<sup>2</sup>, 3.8 μC/cm<sup>2</sup>, and 2.9 μC/cm<sup>2</sup> were reported for (BA)<sub>2</sub>PbCl<sub>4</sub> (*T*<sub>c</sub> = 328 K) [50], (BA)<sub>2</sub>CsPb<sub>2</sub>Br<sub>7</sub> (*T*<sub>c</sub> = 421 K) [53], (BA)<sub>2</sub>(MA)Pb<sub>2</sub>Br<sub>7</sub> (*T*<sub>c</sub> = 352 K) [56], (BA)<sub>2</sub>(NH<sub>2</sub>CHNH<sub>2</sub>)Pb<sub>2</sub>Br<sub>7</sub> (*T*<sub>c</sub> = 322 K) [57], and (BA)<sub>2</sub>(MA)Pb<sub>3</sub>Br<sub>10</sub> (*T*<sub>c</sub> = 315 K) [58], respectively.

Figure 2 illustrates the III ferroelectricity mechanism, where the order–disorder transition of the *n*-BA cation is coupled to the deformation of the inorganic cage to give rise to ferroelectricity. Let us examine (BA)<sub>2</sub>CsPb<sub>2</sub>Br<sub>7</sub> as an example (Figure 2A–D). Although the distortion in the inorganic cesium–lead halide partly lowers its symmetry from cubic to orthorhombic (*Pnma*), that alone

a new way to manipulate the magnetization of magnetic nanostructures by a spin-polarized current. Electron spin orientation and its associated magnetic moment is used as a state variable in the device.



## Trends in Chemistry

**Figure 2.** Paraelectric–ferroelectric transition driven by the concerted motions of  $\text{BA}^+$  organic cations and the inorganic anion cage in 2D hybrid perovskites. (A)  $(\text{BA})_2\text{CsPb}_2\text{Br}_7$  at the paraelectric phase (PEP) viewed along the  $b$ -axis. (B) Corresponding  $\text{PbBr}_6$  octahedra with  $\text{Cs}^+$  at the PEP. (C)  $(\text{BA})_2\text{CsPb}_2\text{Br}_7$  at the ferroelectric phase (FEP). (D) Corresponding  $\text{PbBr}_6$  with  $\text{Cs}^+$  at the FEP. (E)  $(\text{BA})_2(\text{MA})\text{Pb}_2\text{Br}_7$  at the FEP viewed along the  $b$ -axis. (F) Corresponding  $\text{PbBr}_6$  framework with  $\text{MA}^+$  at the FEP. (G)  $(\text{BA})_2(\text{MA})\text{Pb}_2\text{Br}_7$  at the PEP. (H) Corresponding  $\text{PbBr}_6$  octahedra with  $\text{MA}^+$  at the PEP. The yellow arrows indicate the direction of spontaneous electric polarization. (A–D) Adapted, with permission, from [53]; (E–H) adapted, with permission, from [56].

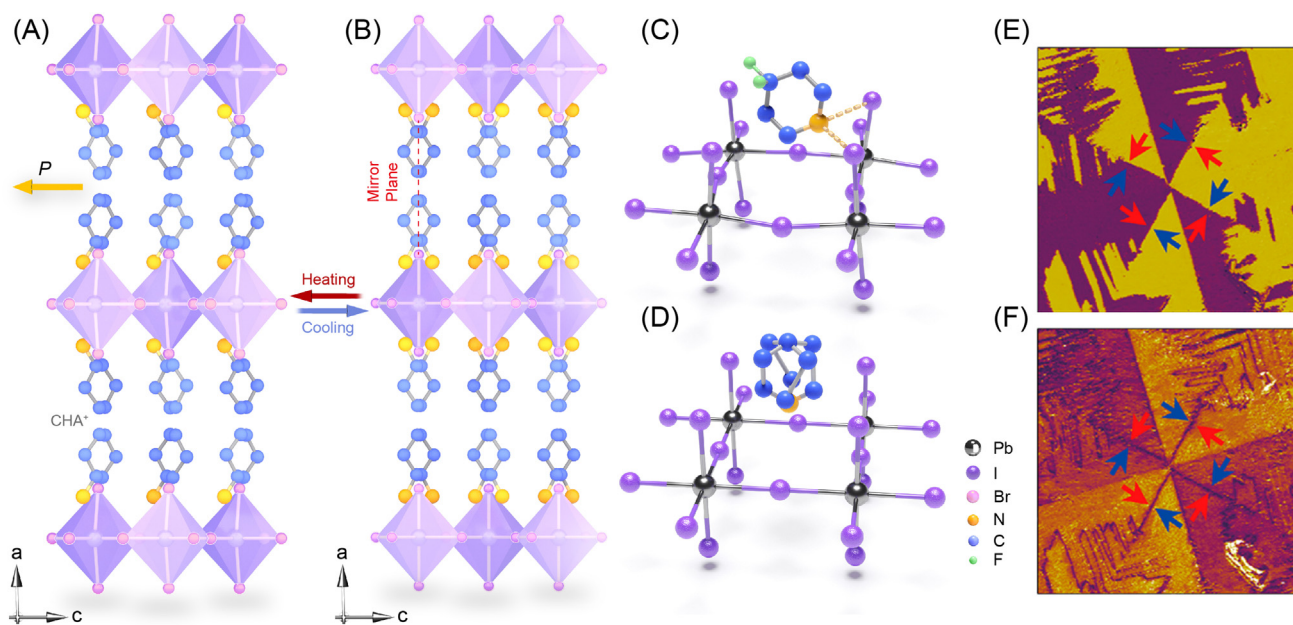
does not guarantee ferroelectricity due to the random arrangement of the dipoles. The alloying of flexible organic cations into the pure inorganic cesium–lead halide perovskite is needed to produce macroscopic polarization. In  $(\text{BA})_2\text{CsPb}_2\text{Br}_7$ , the inorganic  $\text{Cs}^+$  ions and organic  $\text{BA}^+$  cations are displaced along the  $c$ -axis, while the  $\text{N}\text{--}\text{H}\cdots\text{Br}$  hydrogen bond causes the deformation of the  $\text{PbBr}_6$  octahedral cage and the displacement of the negative charges from their center positions. The combination of these motions leads to the separation of negative and positive charges along the polar  $c$ -axis, thereby generating spontaneous polarization. In the high-temperature phase (HTP), the dynamic motion of the  $n$ -BA cation causes the carbon and nitrogen atoms to be distributed symmetrically over two equivalent sites, creating a crystallographic mirror plane (Figure 2A). The  $\text{Cs}^+$  ion is also located in a mirror plane and the  $\text{PbBr}_6$  group adopts a regular octahedral configuration with a highly symmetric conformation (Figure 2B); thus,  $(\text{BA})_2\text{CsPb}_2\text{Br}_7$  belongs to the nonpolar space group of  $Cmca$ . The low-temperature phase (LTP) belongs to the polar space group of  $Cmc2_1$ , in which the ordered arrangement that  $n$ -BA adopts leads to the loss of the mirror plane (Figure 2C) and spontaneous polarization (Figure 2D) [53].

The strength of the hydrogen bonds in 2D hybrid perovskite follows the order  $\text{N-H}\cdots\text{Cl} > \text{N-H}\cdots\text{Br} > \text{N-H}\cdots\text{I}$ . The strong hydrogen bonding in  $(\text{BA})_2\text{PbCl}_4$  gives rise to strong electron–phonon coupling and distortion of the  $\text{PbCl}_4^{2-}$  octahedron, leading to off-centering displacement of the polar center [50]. For higher-homolog RPPs of  $n > 1$ , the spontaneous polarization is driven by the concerted motions of both the small ( $\text{MA}^+$ ) and large ( $\text{BA}^+$ ) cations, whereby hydrogen bonding interactions are important to order both of these cations [56]. In the LTP of  $(\text{BA})_2(\text{MA})\text{Pb}_2\text{Br}_7$ , the reorientation of the  $\text{MA}^+$  cation as well as the longer  $\text{BA}^+$  cation causes the positive charge to be displaced along the *c*-axis in one direction and the negative charge of the distorted  $\text{PbBr}_4^{2-}$  octahedron to be displaced in the opposite direction, giving rise to polarization along the *c*-axis (Figure 2E,F). In the HTP, both  $\text{MA}^+$  and  $\text{BA}^+$  become highly disordered with a symmetric mirror geometry along the *c*-axis while the  $\text{PbBr}_6$  octahedron becomes highly symmetric, causing the polarization to be cancelled (Figure 2G,H). Interestingly, ferroelectricity manifests in the  $\text{PbCl}_6$  or  $\text{PbBr}_6$  framework, but not the  $\text{PbI}_6$  one [59]. This is associated with the greater distortion of the octahedral cage by more electronegative elements, which is reflected by the difference in bond lengths between axial and equatorial  $\text{Pb-X}$  bonds and the tilting of the bond angles. The stronger hydrogen bonds formed by the more electronegative elements also provide stronger coupling with the order–disorder motions of the long organic cations.

#### Aromatic and cyclic organic molecules

Besides linear organic chains, aromatic and cyclic organic molecules like benzylammonium and cyclohexylammonium (CHA) have also been used respectively as organic cations in 2D RPPs. Compared with linear organic cations, the  $P_s$  values are typically higher; for example,  $P_s$  values of  $13 \mu\text{C}/\text{cm}^2$  and  $6.5 \mu\text{C}/\text{cm}^2$  were reported for  $(\text{benzylammonium})_2\text{PbCl}_4$  ( $T_c = 438 \text{ K}$ ) [60] and  $(\text{CHA})_2\text{PbBr}_4$  ( $T_c = 393 \text{ K}$ ), respectively [59]. The type III ferroelectric–paraelectric transition in both is accompanied by a structure transition from the polar space group  $Cmc2_1$  at the LTP (room temperature) to the nonpolar space group  $Cmca$  at the HTP.  $(\text{CHA})_2\text{PbBr}_4$  has a band gap of 2.096 eV, similar to that of  $\text{BiFeO}_3$  [15]; thus, it can be potentially used as a ferroelectric insulator to switch semiconductor channels.  $(\text{CHA})_2\text{PbBr}_4$  is used as an example to discuss the order–disorder transition. As shown in Figure 3A, all of the C–N bonds of the CHA cations align along the *c*-axis at the LTP to give rise to spontaneous polarization. At the HTP, the CHA cations become disordered, resulting in the loss of asymmetry (Figure 3B). The ordering of the CHA cation leads to a 0.82-Å shift of the positive charge and that contributes about  $5.1 \mu\text{C}/\text{cm}^2$ . The rest of  $P_s$  is attributed to the distortion of  $\text{PbBr}_6$  and the displacement of its negative charges in the opposite direction to the CHA. Similarly, in the case of  $(\text{benzylammonium})_2\text{PbCl}_4$ , the ferroelectric LTP can be understood in terms of the ordering of the benzylammonium cation by rotation around the twofold axis and coherent displacement of the inorganic part.

Ferroelectric polarization vectors can order rectilinearly as well as in circles or toroids. The observation of vortex domains has been attributed to a finite size effect or boundary conditions, but the chemical design principle that leads to linear or toroidal ferroelectric domains in 2D hybrid perovskites is not well understood. Recently, a robust ferroelectric vortex–antivortex domain structure was identified in  $(4,4\text{-DFPD})_2\text{PbI}_4$  (4,4-difluoropiperidinium), with a  $P_s$  value of  $10 \mu\text{C}/\text{cm}^2$  and  $T_c$  of 428.5 K, by applying H/F substitution to non-ferroelectric  $(\text{PD})\text{PbI}_3$  (Figure 3C,D) [61]. Piezoresponse force microscopy (PFM) in  $(4,4\text{-DFPD})_2\text{PbI}_4$  reveals exotic quadrant-like domain patterns with the boundaries of eight subdomains merging at one point, forming a topological eightfold domain texture (Figure 3E,F). Electrically switchable vortices are exciting because they can potentially store a high density of memory bits. The flexibility of molecular design in 2D perovskites allows the design of multi-axial ferroelectrics with multiple polarization directions, leading to the formation of domain walls with different angles. These may offer a strategy to study complex domain structures.



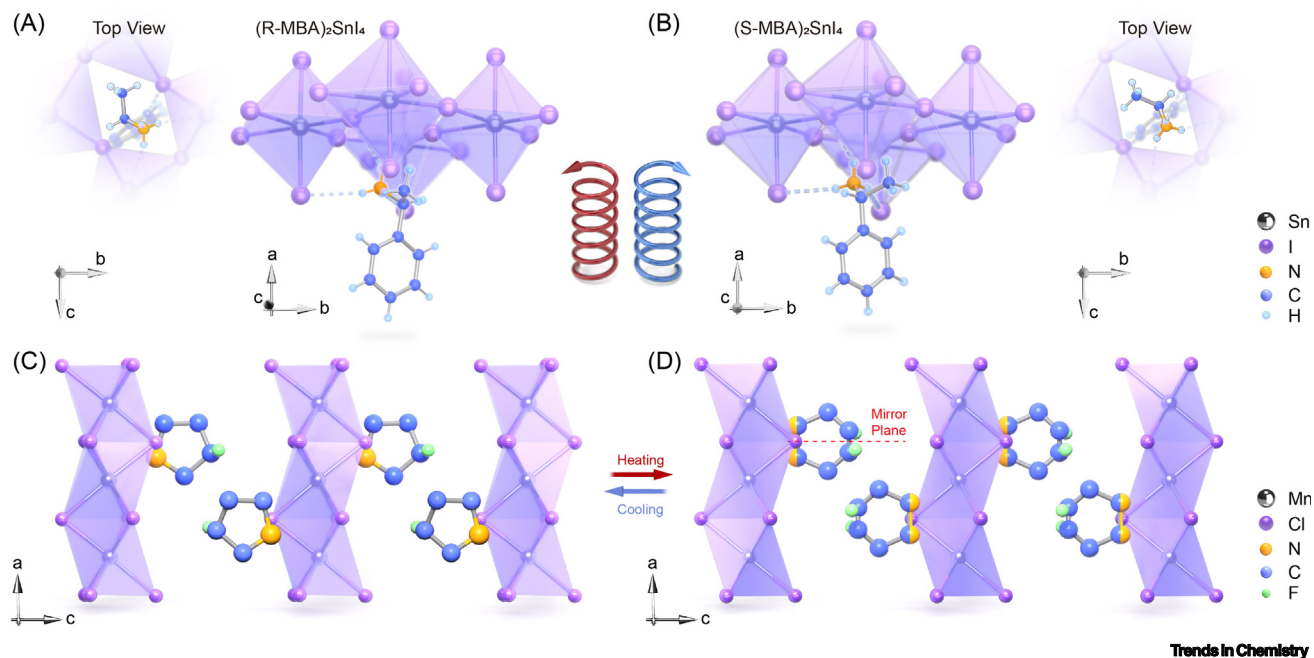
## Trends in Chemistry

**Figure 3. Ferroelectric phase (FEP)–paraelectric phase (PEP) transition of 2D hybrid perovskites.** (A) Perspective view along the *b*-axis of  $(\text{CHA})_2\text{PbBr}_4$  (CHA = cyclohexylammonium) at the FEP. (B) Perspective view of  $(\text{CHA})_2\text{PbBr}_4$  at the PEP. The yellow arrow indicates the spontaneous electrical polarization. (C) Structural unit of  $(4,4\text{-DFPD})_2\text{PbI}_4$  (DFPD = difluoropiperidinium) at the FEP. The N–H...I hydrogen bonds are depicted as broken lines. (D) Structural unit of  $(4,4\text{-DFPD})_2\text{PbI}_4$  at the PEP. (E) Lateral piezoresponse force microscopy (PFM) amplitude image of  $(4,4\text{-DFPD})_2\text{PbI}_4$ . (F) Lateral PFM phase image of  $(4,4\text{-DFPD})_2\text{PbI}_4$ . (A,B) Adapted, with permission, from [59]; (C–F) adapted, with permission, from [61].

## Chiral chains

Incorporating chiral organic molecules into hybrid 2D perovskite imparts spin-filter properties on the layered structure when charge is injected vertically because of chirality-induced spin selectivity [62]. The embedded chiral organic moieties also induce a chirality-dependent optical response from the inorganic metal–halide sublattice. For example, in tin iodide perovskites templated by chiral (*R/S*-)methylbenzylammonium (*R/S*-MBA) [i.e.,  $(\text{R/S-MBA})_2\text{SnI}_4$ ] [63], circularly polarized absorption by the Sn–I lattice was observed (Figure 4A,B). In addition, spin polarization in the current–voltage characteristics of as high as 94% could be obtained. This was demonstrated using magnetic conductive probe spectroscopy, where the vertical current through the sample was measured for different tip magnetizations. The spin-filtering properties of 2D chiral perovskite had also been demonstrated in (*R/S*-*rac*-)methylbenzylammonium lead iodide (*R/S*-*rac*-MBA) $_2\text{PbI}_4$  [64], where the spin selectivity results from spin-polarized tunnel barriers formed by the chiral organic layers. The spin selectivity increases with the chiral barrier layers, suggesting that chiral 2D hybrid perovskites can serve both as a spin-filter and a tunneling barrier.

Chiral 2D hybrid perovskites form enantiomorphic crystals adopting the five chiral polar point groups  $C_1$ ,  $C_2$ ,  $C_3$ ,  $C_4$ , and  $C_6$  to obtain intrinsic ferroelectric properties [65]. For example, homo-chiral organic cations of 1-(4-chlorophenyl)ethylammonium have been incorporated into 2D lead iodide perovskite to form enantiomers of [*R*-1-(4-chlorophenyl)ethylammonium] $_2\text{PbI}_4$  (*R*-LIPF) (Figure 1C) and [*S*-1-(4-chlorophenyl)ethylammonium] $_2\text{PbI}_4$  (*S*-LIPF). At room temperature, both of these crystallize in the  $P1$  space group belonging to the chiral polar point group  $C_1$  [49]. A  $P_s$  value of  $13.96 \mu\text{C}/\text{cm}^2$  was reported for *R*-, and *S*-LIPF, with  $T_{c(R)} = 483 \text{ K}$  and  $T_{c(S)} = 473.2 \text{ K}$ . The single-chlorine substitution in the organic cation enhances the electric dipole moment owing to the strong electronegativity;  $T_c$  was also increased due to enhanced intermolecular



Trends in Chemistry

**Figure 4.** Structural comparison of chiral hybrid perovskites. (A) Crystal structure of (*R*-methylbenzylammonium)<sub>2</sub>SnI<sub>4</sub> with absorption of left-handed circularly polarized light. (B) Crystal structure of (*S*-methylbenzylammonium)<sub>2</sub>SnI<sub>4</sub> with absorption of right-handed circularly polarized light. (C) Crystal structure of (*R*)-3-(fluoropyrrolidinium)MnCl<sub>3</sub> at the ferroelectric phase (FEP) and (D) crystal structure of (*R*)-3-(fluoropyrrolidinium)MnCl<sub>3</sub> at the paraelectric phase (PEP). (A,B) Adapted, with permission, from [63]; (C,D) adapted, with permission, from [69].

interaction [66]. Ferroelectric polarization in chiral hybrid perovskites originates mainly from the order–disorder transition of the homochiral cations. This is illustrated in the enantiomeric perovskite ferroelectric (*R*)- and (*S*)-3-(fluoropyrrolidinium)MnCl<sub>3</sub>. (Pyrrolidinium)MnCl<sub>3</sub> itself exhibits ferroelectricity, with  $T_c$  of 295 K [67,68]. After single-fluorine substitution, the  $T_c$  increased to 333 K with  $P_s$  values of 4.83  $\mu\text{C}/\text{cm}^2$  and 4.84  $\mu\text{C}/\text{cm}^2$  in (*R*)- and (*S*)-3-(fluoropyrrolidinium)MnCl<sub>3</sub>, respectively [69]. The positive charge of chiral cations is located on the N atoms. As shown in Figure 4C, the well-ordered enantiomeric 3-fluoropyrrolidinium cations form linear chains of face-sharing MnCl<sub>6</sub> octahedra, and the overall structure adopts the chiral-polar space group  $P2_1$ . In the HTP, the N atom in the organic cation displaces to the center of the twofold axis, which makes the 3-fluoropyrrolidinium cation orientationally disordered with the twofold axis (Figure 4D). This causes it to adopt the nonpolar chiral space group  $C222_1$ .

### Design strategies

The rational design and synthesis of 2D hybrid perovskite ferroelectrics has gained considerable traction recently [70–73]. The strategies pioneered by the groups of Xiong and colleagues as well as Luo and colleagues generally involve the introduction of distortion or structural asymmetry in the inorganic anion cage or organic cation, as well as an increase in the strength of hydrogen bonding between the organic and inorganic moieties. The coherent motion between the organic and inorganic moieties can be described as a coupling of the ordering of the organic cation with the asymmetry of the inorganic anionic cage at the ferroelectric phase, versus the coupling of the disorder of the organic cations with the symmetry of the inorganic anionic cage. In addition, to couple the momentum of the organic and inorganic moieties, it is important to match the cations and anions in terms of their size, mass, and intermolecular interactions to modulate the ferroelectricity [55]. One intuitive way of viewing this is to imagine the long organic cations as ‘ropes’ slowing the molecular rotation of the inorganic moieties.

An interesting illustration of the ‘momentum-matching’ concept is the case of  $[(\text{CH}_3)_4\text{N}]\text{PbI}_3$ , a non-polar hybrid perovskite. The question is whether halogen substitution to form  $[(\text{CH}_3)_3\text{NCH}_2\text{X}]\text{PbI}_3$ , where X = halogen, can introduce ferroelectricity. Unlike the previous case where the use of the more electronegative F atom causes stronger hydrogen bonding and hence greater polarization, ferroelectricity in this case is determined by matching the size and weight between the organic cation and the  $[\text{PbI}_3]^-$  anion. The larger-sized  $[(\text{CH}_3)_3\text{NCH}_2]^+$  affords stronger  $[(\text{CH}_3)_3\text{NCH}_2]\cdots\text{I}$  halogen bonding with the  $[\text{PbI}_3]^-$  anion compared with the  $(\text{CH}_3)_3\text{NCH}_2\text{F}^+$ ,  $(\text{CH}_3)_3\text{NCH}_2\text{Cl}^+$ , and  $(\text{CH}_3)_3\text{NCH}_2\text{Br}^+$  cations [66]. Thus, ferroelectricity is detected in  $[(\text{CH}_3)_3\text{NCH}_2]\text{PbI}_3$  only because effective momentum between the cation and anion prevents the tumbling motion of the organic cation that breaks the asymmetry.

### In-plane and out-of-plane ferroelectricity in hybrid perovskites

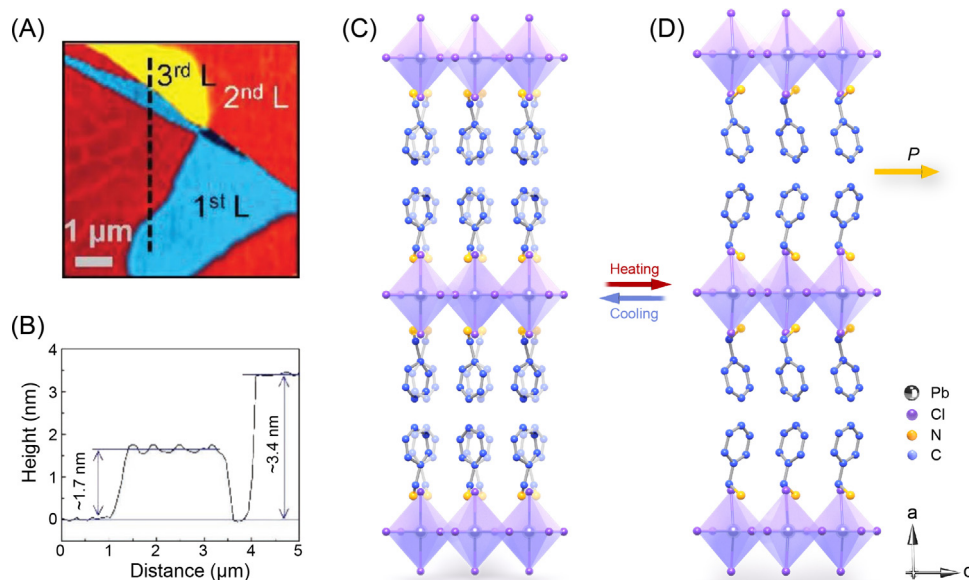
In traditional perovskite-structure ferroelectric oxides such as  $\text{PbTiO}_3$  and  $\text{BaTiO}_3$ , the out-of-plane polarization originates from the vertical off-center ordering or displacement of cations from the centrosymmetric position [74–76]. Due to a depolarization effect, the ferroelectricity is suppressed at reduced thickness [77]. Such thickness-dependent depolarization may be less pronounced in 2D hybrid perovskites showing in-plane ferroelectricity because of the weak or absent interlayer coupling arising from the layer-by-layer segregation of the organic and inorganic layers. However, interfacial strain effects may disturb the subtle ordering of the organic cations, which can affect the ferroelectricity [78]. Further studies are needed to verify whether ferroelectricity can be sustained down to single-quantum-well levels in the layered hybrid perovskites.

#### In-plane ferroelectricity in thin 2D hybrid perovskites

Most ferroelectric RPPs show in-plane polarization arising from the dipoles associated with the ammonium ions. In-plane ferroelectricity has been reported in molecularly thin  $(\text{benzylammonium})_2\text{PbCl}_4$  hybrid 2D perovskites [79] (Figure 5A,B). Essentially, the horizontal off-center ordering of the  $\text{RNH}_3^+$  with respect to the inorganic framework results in in-plane polarization. To understand how spontaneous in-plane polarizations arise in RPPs, we have selected as an example  $(\text{benzylammonium})_2\text{PbCl}_4$ , which has a mixed character of order–disorder and displacive-type ferroelectrics (type III). As shown in Figure 5C, corner-sharing  $\text{PbCl}_6$  octahedra occupy the mirror plane parallel to the  $bc$  plane. The HTP is centrosymmetric, with disordered benzylammonium locating at the twofold screw axis perpendicular to the  $bc$  plane. Below  $T_c$ , the organic cation is frozen in one of the two off-center positions with the N atom aligned uniformly along the  $c$ -axis direction (Figure 5D). This leads to in-plane spontaneous polarization parallel to the mirror plane along the  $c$ -axis direction. According to density functional theory (DFT) calculations of the total polarization in  $(\text{benzylammonium})_2\text{PbCl}_4$  by considering the correlated distortions of the organic and inorganic framework, two-thirds of the total polarization are attributed to the organic cations, with one-third attributable to the inorganic parts [80]. This appears to be applicable to most 2D hybrid perovskites; thus, the organic cation plays major role in the ferroelectricity.

#### Out-of-plane ferroelectricity in 2D Dion–Jacobson (D–J) perovskite

In **D–J 2D hybrid perovskites**, the van der Waals gap is replaced by diammonium cations [81–83]; thus, the interlayers are held by ionic bonds. Loh and colleagues have recently demonstrated that D–J perovskites of the formula  $(\text{AMP})\text{PbI}_4$  [where AMP is 4-(aminomethyl)piperidinium] have both ferroelectricity and a Rashba effect, with  $P_s$  of  $9.8 \mu\text{C}/\text{cm}^2$  ( $T_c = 352 \text{ K}$ ) [84]. As shown in Figure 6A, the unit cell of the ferroelectric phase has two  $\text{AMP}^{2+}$  cations oriented alternately in an ‘up-and-down’ configuration in the interlayer of  $[\text{PbI}_4]^{2-}$ ; the asymmetric configuration gives rise to vertical off-center polarization in the out-of-plane direction. Above  $T_c$ , the AMP molecules are located at the inversion center, causing the polarization to be canceled (Figure 6B). DFT calculations reveal that the organic  $\text{AMP}^{2+}$  cations contribute  $10.34 \mu\text{C cm}^{-2}$  while the inorganic  $[\text{PbI}_4]^{2-}$  framework

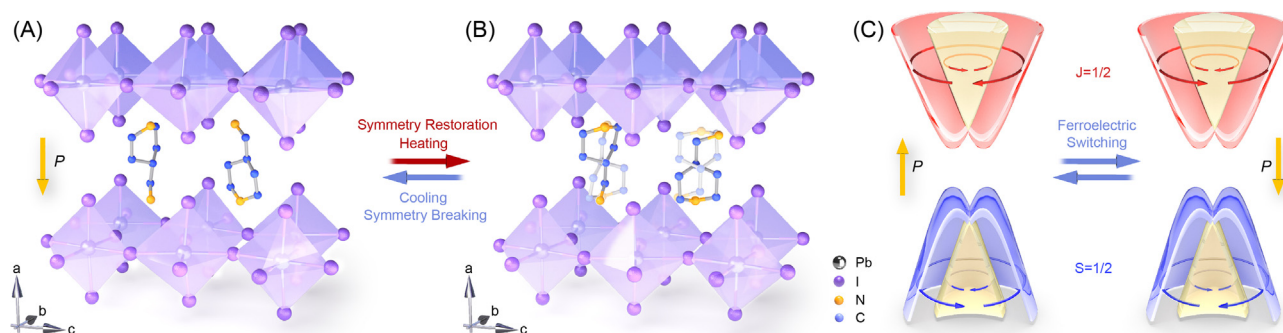


## Trends in Chemistry

**Figure 5.** In-plane ferroelectricity in thin 2D hybrid perovskite of  $(\text{benzylammonium})_2\text{PbCl}_4$ . (A) Atomic force microscopy (AFM) image of thin  $(\text{benzylammonium})_2\text{PbCl}_4$  flakes of differing thickness. (B) Corresponding height profile along the black broken line in (A). (C) Perspective view of  $(\text{benzylammonium})_2\text{PbCl}_4$  at the ferroelectric phase (FEP). (D) Perspective view of  $(\text{benzylammonium})_2\text{PbCl}_4$  at the paraelectric phase (PEP). The in-plane spontaneous polarization is along the *c*-axis with the demonstration of the N atom indicated as a yellow arrow. (A–D) Adapted, with permission, from [79].

contributes  $0.59 \mu\text{C cm}^{-2}$ , demonstrating that the AMP cations contribute almost all of the total polarization [85].

The practical implementation of ferroelectric devices requires low-power and low-voltage operation. Dynamic domain behavior and the movement of domain boundaries are elementary processes in polarization reversal and their imaging will be highly useful in understanding ferroelectric switching process. Although high-resolution ( $\approx 10$  nm) imaging of static domain structures on hybrid perovskites has been routinely performed using PFM, there are few real-time studies of domain-switching dynamics on the nanoscale. In many ferroelectric oxides, the movement of ferroelectric domains is



## Trends in Chemistry

**Figure 6.** Out-of-plane ferroelectricity and Rashba effect in Dion–Jacobson 2D hybrid perovskite. (A) Asymmetrical crystal structure of  $(\text{AMP})\text{PbI}_4$  crystal [AMP = 4-(aminomethyl)piperidinium] at the ferroelectric phase (FEP). The out-of-plane spontaneous polarization is along the *a*-axis. (B) Symmetrical crystal structure of  $(\text{AMP})\text{PbI}_4$  at the paraelectric phase (PEP). (C) Schematic illustration of ferroelectric switching of the Rashba effect in Rashba ferroelectric perovskites. The helicity is inverted on ferroelectric switching. (A,B) Adapted, with permission, from [84]; (C) adapted, with permission, from [37].

coupled to strain-related phase change or orientation shift (i.e., ferroelasticity). Ferroelasticity represents material domains possessing spontaneous strain that can be switched by external stress, and a ferroelastic phase transition can occur without ferroelectricity. Xun Xiao *et al.* suggests that the ferroelasticity originates from the breaking of strain equivalence in a and b lattice constants by the rotation of the aspherical methyl ammonium molecules in 2D RPP perovskites; thus, ferroelasticity is observed only for  $n > 1$  homologs [3]. There is no report to date investigating whether the ferroelectric domain switching in hybrid perovskites is assisted by ferroelastic domain walls. Ferroelectric domain walls with a potential gradient provide pathways for the separation of photogenerated electron-hole pairs, leading to reduced recombination loss [86,87]. A recent PFM study, however, questioned the previous assignments of 1D stripes on 3D hybrid perovskites as ferroelectric domains and argued that these are ferroelastic domains instead because they cannot be switched electrically, but can be switched by stress [2]. By contrast, evidence for electrically switchable ferroelectric domains on 2D hybrid perovskites is more solid, as electrically switchable PFM phase and amplitude images of the domains are often presented [88]. Ferroelectric polarization vectors can order rectilinearly as well as in circles or toroids. The observation of vortex domains has been attributed to a finite size effect or boundary conditions, but the chemical design principle that leads to linear or toroidal ferroelectric domains in 2D hybrid perovskites is not well understood.

### Ferroelectric Rashba 2D perovskites for spintronics

From the viewpoint of electrically switchable spin devices, it is highly useful for a material to possess both ferroelectricity and Rashba spin-split properties, such that an electrically tunable Rashba effect can be achieved (Box 1). Ferroelectric hybrid perovskite materials are necessarily bulk inversion asymmetric and thus the SOCs are Dresselhaus type, as opposed to interface Rashba-Edelstein SOCs in centrosymmetric materials. A combination of both interface and bulk Rashba effects is possible for 2D perovskites that are interfaced to other semiconductors. Here, we denote 2D hybrid perovskites that possess ferroelectric properties as bulk Rashba materials because the absence of inversion symmetry is implicit and SOC is ensured by the heavy atoms (e.g., Pb, Sn, I) in the inorganic anion cage. The spin splitting in Rashba materials causes the band maxima to move in k-space and give rise to unusual magneto-optical effects [89] as well as bright triplet emissions [90]. The strength of the Rashba effect can be quantified through the k-space shift  $k_R$ , the Rashba energy  $E_R$ , and the 'Rashba parameter'  $\alpha_R$ . An example of bulk Rashba and ferroelectric materials is 2D D-J perovskites, (AMP)PbI<sub>4</sub>, as mentioned before. Circularly polarized PL studies of (AMP)PbI<sub>4</sub> revealed giant Rashba splitting of 85 meV and a Rashba coefficient  $\alpha$  of 2.6 eV Å at room temperature [84], which is of the same order as BiTeI and GeTe and much larger than III-V semiconductors such as GaAs [1].

The Rashba parameter in 2D hybrid perovskites is typically larger than that reported for 3D hybrid perovskites. The calculated Rashba coefficient of a 2D hybrid perovskite is about eight times larger than that of a 3D MAPbI<sub>3</sub> hybrid perovskite based on experimental second-harmonic-generation results and their correlations to structural inversion symmetry breaking [91]. Magnetoconductance (MC) and magneto-electroluminescence (MEL) studies on a light-emitting diode (LED) made of (BA)<sub>2</sub>(MA)Pb<sub>2</sub>I<sub>7</sub> reported a Rashba coefficient that was about seven times larger than that for MAPbI<sub>3</sub>; the applied magnetic field directly manipulates the spin precession of charge carriers and alters the spin mixing rate between loosely bound singlet and triplet excitons [92]. The peak widths in MC and MEL were found to be proportional to the spin-interaction energy in the emissive layers in hybrid perovskites.

### Measuring Rashba SOC

The correlation between the spin coherence dynamics and layer thickness ( $n$ ) in 2D hybrid perovskites of the formula (PEA)<sub>2</sub>(MA) <sub>$n-1$</sub> Pb <sub>$n$</sub> I <sub>$3n+1$</sub>  has been investigated using circularly polarized pump

### Box 1. Ferroelectric Rashba 2D perovskites for spintronics

Ferroelectric Rashba 2D perovskites allow all-electrical control of spin transport. The spin-dependent deflection of electron trajectories in the presence of a spin orbit split band structure gives rise to spin accumulation at edges [117] (Figure 1A). For systems lacking inversion symmetry, like ferroelectric Rashba 2D perovskites, spin-polarized electrons moving along the x-axis experience an effective Rashba field  $B_{Ry}$  along the y-axis and undergo spin precession [118] (Figure 1B). The strength of the Rashba field and spin precession can be controlled by a gate voltage,  $E_z$ . Recent theoretical work predicts that switching ferroelectric polarization in the 2D D-J (AMP)PbI<sub>4</sub> perovskite not only inverts the spin texture chirality but also interchanges the major and minor axes of the Rashba anisotropy ellipse in k-space [85] (Figure 1C). Spin-polarized electrons injected into the ferroelectric Rashba 2D perovskite channel from a ferromagnetic electrode undergo precession under the influence of a Rashba effective magnetic field. The spin-to-charge conversion by the **inverse Edelstein effect** can be detected as a non-local transverse Hall voltage [119] as shown in Figure 1D.

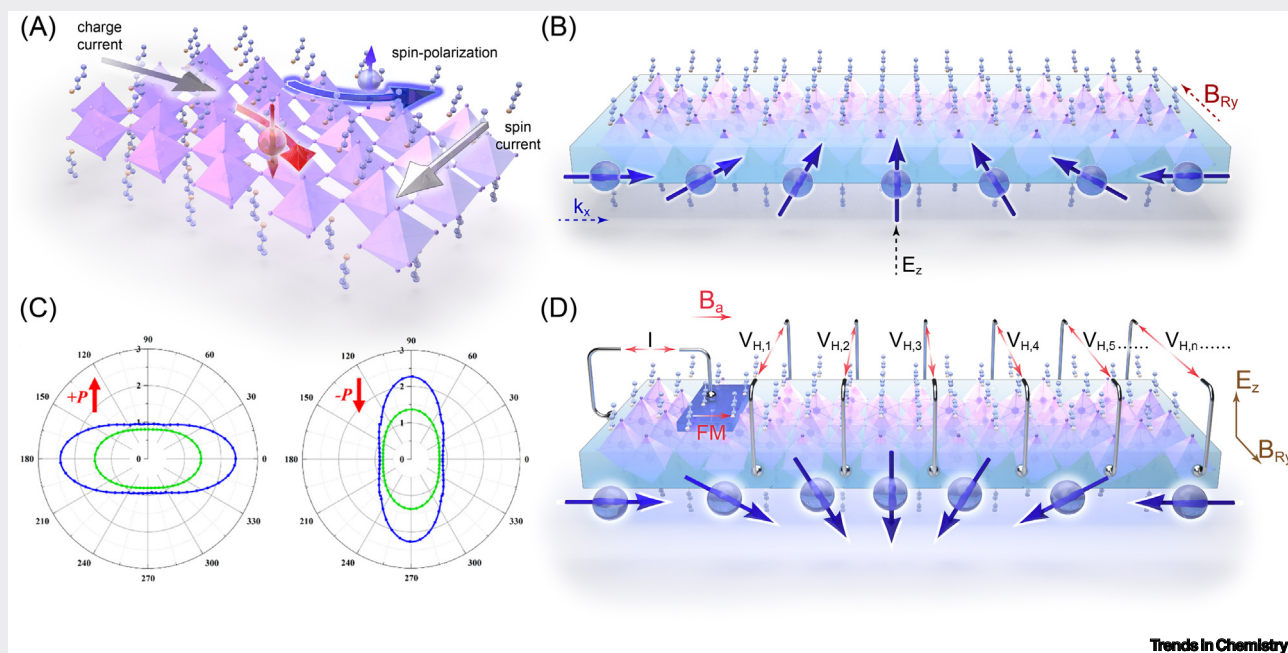


**Figure 1. Spin generation, manipulation, and detection in ferroelectric Rashba 2D perovskites.** (A) Charge-to-spin conversion in a 2D perovskite. (B) Spin-polarized electrons along the x-axis experience an in-plane Rashba field  $B_{Ry}$  along the y-axis, resulting in spin precession. (C) Electrically switchable Rashba anisotropy. (D) Spin-polarized electrons injected via a ferromagnetic electrode into the 2D perovskite channel undergo spin precession as the Rashba magnetic field is perpendicular to the spin polarization, and a nonlocal spin Hall voltage can be detected. (B) Adapted, with permission, from [118]; (C) adapted, with permission, from [85]; (D) adapted, with permission, from [119].

and probe pulses [93]. The change in spin lifetime with layer thickness is not monotonic; it increases with layer thickness from  $n = 1$  to  $n = 4$  because of the decreased phonon-scattering process, followed by a decrease from  $n = 4$  to  $\infty$  (3D). The longer spin lifetime in 2D hybrid perovskites compared with 3D hybrid perovskites is explained by the stronger Rashba effect in the layered system. The longest coherence lifetime of  $\sim 7$  ps is reported in the  $n = 4$  (PEA)<sub>2</sub>(MA) <sub>$n-1$</sub> PbI<sub>3 $n+1$</sub>  and such a long spin lifetime is surprising in view of its large SOC, which usually leads to spin decoherence. In ferroelectric BA<sub>2</sub>PbCl<sub>4</sub> with an in-plane polarization, the spin orbit field was also proposed to have unidirectional out-of-plane alignment. Injected electrons with in-plane spins would therefore precess around the out-of-plane axis, giving rise to a long-lived **persistent spin helix**. In principle, the spin direction in each sub-band can be changed by 180° on the reversal of polarization, thereby allowing its electrical control. This is highly useful for spin-logic devices, in which spin current is manipulated by ferroelectric polarization switching [37] (Figure 6C). The unidirectional spin orbit field is preserved by the crystalline symmetries even when including higher-order spin–momentum coupling terms [80]; this prevents spin decoherence effects based on the **Dyakonov–Perel relaxation mechanism** [94,95], which will help to increase the spin lifetime of the carriers.

The fact that an in-plane ferroelectric 2D hybrid perovskite will have an out-of-plane Rashba spin orbit field driven by its single inversion asymmetry has profound implications; this is analogous to the situation when the Rashba and Dresselhaus terms in a semiconductor quantum well become equal, leading to a unidirectional, field-tunable, large spin orbit field and a momentum-independent spin configuration (i.e., the so-called persistent spin helix). A large anisotropy in 2D D-J perovskites has been predicted by theoretical calculations. The coupling between the ferroelectric polarization and switchable, highly anisotropic Rashba spin-split bands allows not only the spin texture chirality to be inverted as the polarization is reversed, but also the major and minor axes of the Rashba anisotropy ellipse in k-space to be interchanged [85] (Box 1).

In addition, the strong electron–phonon coupling in hybrid perovskites is known to create polarons, which are coherent quasiparticles comprising an electron surrounded by a phonon cloud. The polaron dispersion and effective mass can be significantly renormalized from those of the bare electron band. The interplay between SOC and electron–phonon coupling lift the degeneracy of the two spin-polarized bands, such that one is well described by a long-lived, light quasiparticle while the other is highly incoherent [96]. This will lead to very different conductivities for the two spin polarizations, making such a material an ideal spin source.

#### Realizations of spin orbitronics

The charge current carried by a Rashba material is automatically associated with a nonzero spin density (spin accumulation); the latter can be measured in a spin FET devices or Hall bar devices (Box 1). The case of a centrosymmetric structure exhibiting Rashba spin splitting under the influence of a transverse electric field has been considered theoretically. The spintronics method of accessing the Rashba effect is to probe the charge-to-spin and spin-to-charge conversions based on the spin Hall effect [97] and the inverse-spin Hall effect [98] by building spin Hall effect devices [99]. For example, in the spin-galvanic effect, the electric current can be created either by spin injection or by optical excitation. Spin-polarized carrier injection from ferromagnetic electrodes into MAPbBr<sub>3</sub> has been demonstrated by both optical and electrical means using a spin LED and a vertical spin-valve device, respectively [100]. In the spin LED, circularly polarized electroluminescence was detected. In the spin-valve device, a magnetic field is applied perpendicular to the injected spin orientation to measuring the ‘electrical Hanle effect’, from which a relatively long spin lifetime of 936 ps is obtained. Many electro-optical techniques, such as the **circular photogalvanic effect** [101], polarization- and angle-resolved photoemission spectroscopy (ARPES) [102], transient anisotropy [103], electroabsorption [41], and spin relaxation [104], have also been used to investigate Rashba splitting.

Two main classes of device can be used to exploit the Rashba ferroelectric effect on hybrid perovskites: spin transistors and spin–orbit torque devices. The ‘Datta–Das’ [105] and modified **Datta–Das** [106] transistor architectures allow the possibility of controlling the spin precession in the material using gate-voltage spin FET (Box 1). For spin–orbit torque devices, the nonzero spin density in the Rashba channel generates a spin-transfer torque to switch the magnetization of the magnetic layer interfaced to it. Although Rashba spin splitting in hybrid perovskite has been extensively studied using circularly polarized optical techniques, reports of electrically driven spintronics devices using 2D hybrid perovskites as the spin source or spin channel material are rare. One of the challenges in fabricating electrical devices on 2D hybrid perovskites is the high contact resistance caused by the long organic cations; thus, a tunneling contact has to be used [107].

An enticing prospect is the use of 2D hybrid perovskites as van der Waals-interfaced spin tunneling barriers and spin sources. Traditionally, spin Hall/inverse-spin Hall effects have been

investigated using ferromagnet (FM) spin injectors interfaced to the spin-carrying material [108]. In most cases, the spin conductance mismatch between the spin source and the channel material leads to low spin injection efficiency. Ultrathin metal oxide [108,109] as well as hexagonal boron nitride [110] has been used as a tunneling barrier between the FM spin injector and the channel material to mitigate the conductivity mismatch [111] and enhance the spin injection efficiency. The structure of layered hybrid perovskites is such that they can serve as both spin generation materials and tunneling barriers. The multiple-quantum-well structure of RPPs presents thickness-controllable tunneling barriers; coupled with their large Rashba spin-splitting properties, they can be used in charge–spin interconversion by the Edelstein [97] and inverse Edelstein [98] effects. We have previously shown that despite their high contact resistance, molecularly thin 2D hybrid perovskites form good van der Waals interfaces with graphene, which enables electron tunneling across the interface and electrostatic gating of the perovskite [107]. This suggests the possibility of tuning Rashba SOC in molecularly thin perovskite by electrostatic gating. The high interface resistance of 2D perovskites and the van der Waals gap avoid conductance mismatch when used for spin injection; thus, they can serve as a spin-source material interfaced to a spin-carrying semiconductor.

Most hybrid perovskites synthesized so far have only uniaxial polarization (either in-plane or out-of-plane polarization), which is compatible with the standard two-level storage capacity for binary logic. There is interest in designing 2D hybrid perovskites with multiaxial polarization, in which the multiple ferroelectric axes and equivalent polarization directions allow not only higher storage density but also more effective and easier polarization switching. A biaxial lead halide ferroelectric,  $\text{EA}_4\text{Pb}_3\text{Br}_{10}$  (EA = ethylammonium) with four equivalent polarization directions in the ferroelectric phase [112], as well as the multiaxial ferroelectric [3,3-difluorocyclobutylammonium] $_2\text{CuCl}_4$  with four ferroelectric axes and eight equivalent polarization directions, has been reported [113]. Exceeding these, a multiaxial ferroelectric with 12 polarization directions based on  $[(\text{CH}_3)_3\text{NCH}_2\text{X}]\text{FeBr}_4$  (X = F, Cl, Br, I) was recently reported; these multiaxial ferroelectrics were found to exhibit a relatively large piezoelectric response comparable with that of PVDF [114]. The ability of a multiaxial ferroelectric to show multistable ferroelectric states enables the design of ferroelectric multibit cells (FMBCs) with nontrivial topological access to memory levels by the specific protocol of the applied electric field [115]. The outcome of having a multiaxial polar axis on the spin orbit field has not been considered by theory so far, but we can expect that the spin texture can be changed considerably.

### Concluding remarks

In conclusion, 2D hybrid perovskites are emergent Rashba ferroelectric semiconductors that have the potential to rival inorganic semiconductors. Their flexible chemical design allows inversion asymmetry to be engineered in the structure, which can drive ferroelectricity as well as a unidirectional spin orbit field. One key question is whether we can electrostatically gate 2D hybrid perovskites and tune their spin orbit field. The spin lifetime in 2D perovskites should be measured in systems with and without in-plane ferroelectricity, to see whether the latter can generate a persistent spin helix (see [Outstanding questions](#)). This is particularly important because the utility of spintronics relies on whether the spin polarization of the electron can be maintained for sufficiently long. The Rashba SOC effect in perovskites allows the interconversion of electron and spin currents, which is useful in generating the spin–orbit torque needed to switch the magnetization of the FM. Rashba ferroelectrics in 2D hybrid perovskites afford the alluring possibility of combining a large spin Hall angle (i.e., charge-to-spin conversion efficiency) with coherent spin transport in a single material. At present, we need to determine the charge-to-spin conversion efficiency in 2D hybrid perovskites and investigate how the ferroelectric field can be tapped to improve the spin Hall angle. Another question is whether the layered structure of 2D hybrid

### Outstanding questions

Can we demonstrate electrically switchable spin polarization in 2D hybrid perovskites with Rashba ferroelectric properties?

Can we electrostatically gate 2D hybrid perovskites and tune their spin orbit field?

Can we demonstrate a persistent spin helix in 2D hybrid perovskites with in-plane ferroelectric properties?

What is the charge-to-spin conversion efficiency in 2D hybrid perovskites with Rashba spin-split properties?

Can ferroelectricity remain robust in 2D hybrid perovskites of single-quantum-well thickness?

Can we make multiferroic 2D hybrid perovskites (e.g., ferroelectric and ferromagnetic) and demonstrate magnetoelectric coupling?

Can we use 2D hybrid perovskites in nonvolatile memory elements, logic computation, and semiconductor spintronics?

perovskites allows the ferroelectric polarization and the bulk Rashba parameter to be maintained when the material is scaled down to the thickness of a single quantum well, which is an important advantage in microelectronic devices (see Outstanding questions). Above all, 2D hybrid perovskites serve as a new quantum material platform to study the coupling between SOC and various ferroic orders, including charge, spin, lattice, and strain. Ferromagnetic hybrid perovskites with transition-metal ions such as  $\text{Cu}^{2+}$ ,  $\text{Ni}^{2+}$ ,  $\text{Mn}^{2+}$ , or  $\text{Fe}^{2+}$  bring the prospect of multiferroics combining ferroelectricity and ferromagnetism [116]. The coupling of ferroelectric and magnetic order, mediated by the spin–orbit interaction, offers a rich playground for emergent phenomena in multifunctional materials. Future research should investigate magnetoelectric coupling in these materials and how 2D hybrid perovskites with Rashba ferroelectric properties can be applied in nonvolatile memory elements, logic computation, and semiconductor spintronics (see Outstanding questions).

### Acknowledgments

K.L. acknowledges funding support from the Start-up Fund for RAPs under the Strategic Hiring Scheme, Grant No. P0036112, The Hong Kong Polytechnic University. K.P.L. acknowledges funding support from Singapore's Ministry of Education Tier 2 Grant MOE2019-T2-1-037.

### Declaration of Interests

The authors have no interests to declare.

### References

- Picozzi, S. (2014) Ferroelectric Rashba semiconductors as a novel class of multifunctional materials. *Front. Phys.* 2, 10
- Strelcov, E. *et al.* (2017)  $\text{CH}_3\text{NH}_3\text{PbI}_3$  perovskites: ferroelasticity revealed. *Sci. Adv.* 3, e1602165
- Xiao, X. *et al.* (2021) Layer number dependent ferroelasticity in 2D Ruddlesden–Popper organic–inorganic hybrid perovskites. *Nat. Commun.* 12, 1332
- Pandey, R. *et al.* (2019) Mutual insight on ferroelectrics and hybrid halide perovskites: a platform for future multifunctional energy conversion. *Adv. Mater.* 31, 1807376
- Kreisel, J. *et al.* (2012) A photoferroelectric material is more than the sum of its parts. *Nat. Mater.* 11, 260
- Lu, H. *et al.* (2012) Mechanical writing of ferroelectric polarization. *Science* 336, 59
- Scott, J.F. (2007) Applications of modern ferroelectrics. *Science* 315, 954
- Spaldin, N.A. and Ramesh, R. (2019) Advances in magnetoelectric multiferroics. *Nat. Mater.* 18, 203–212
- Boyn, S. *et al.* (2017) Learning through ferroelectric domain dynamics in solid-state synapses. *Nat. Commun.* 8, 14736
- Chanthbouala, A. *et al.* (2012) A ferroelectric memristor. *Nat. Mater.* 11, 860–864
- Fiebig, M. *et al.* (2016) The evolution of multiferroics. *Nat. Rev. Mater.* 1, 16046
- Choi, T. *et al.* (2009) Switchable ferroelectric diode and photovoltaic effect in  $\text{BiFeO}_3$ . *Science* 324, 63
- Grinberg, I. *et al.* (2013) Perovskite oxides for visible-light-absorbing ferroelectric and photovoltaic materials. *Nature* 503, 509–512
- Seidel, J. *et al.* (2011) Efficient photovoltaic current generation at ferroelectric domain walls. *Phys. Rev. Lett.* 107, 126805
- Yang, S.Y. *et al.* (2010) Above-bandgap voltages from ferroelectric photovoltaic devices. *Nat. Nanotechnol.* 5, 143–147
- Shi, P.-P. *et al.* (2019) Two-dimensional organic–inorganic perovskite ferroelectric semiconductors with fluorinated aromatic spacers. *J. Am. Chem. Soc.* 141, 18334–18340
- Shi, C. *et al.* (2020) Two-dimensional organic–inorganic hybrid rare-earth double perovskite ferroelectrics. *J. Am. Chem. Soc.* 142, 545–551
- Yang, T.-Y. *et al.* (2015) The significance of ion conduction in a hybrid organic–inorganic lead-iodide-based perovskite photosensitizer. *Angew. Chem. Int. Ed.* 54, 7905–7910
- Sharada, G. *et al.* (2016) Is  $\text{CH}_3\text{NH}_3\text{PbI}_3$  polar? *J. Phys. Chem. Lett.* 7, 2412–2419
- Chen, X.-G. *et al.* (2020) Confinement-driven ferroelectricity in a two-dimensional hybrid lead iodide perovskite. *J. Am. Chem. Soc.* 142, 10212–10218
- Hou, Y. *et al.* (2020) Two-dimensional hybrid organic–inorganic perovskites as emergent ferroelectric materials. *J. Appl. Phys.* 128, 060906
- Li, L. *et al.* (2020) A potential Sn-based hybrid perovskite ferroelectric semiconductor. *J. Am. Chem. Soc.* 142, 1159–1163
- Leng, K. *et al.* (2018) Molecularly thin two-dimensional hybrid perovskites with tunable optoelectronic properties due to reversible surface relaxation. *Nat. Mater.* 17, 908–914
- Grancini, G. and Nazeeruddin, M.K. (2019) Dimensional tailoring of hybrid perovskites for photovoltaics. *Nat. Rev. Mater.* 4, 4–22
- Smith, M.D. *et al.* (2018) The diversity of layered halide perovskites. *Annu. Rev. Mater. Res.* 48, 111–136
- Smith, I.C. *et al.* (2014) A layered hybrid perovskite solar-cell absorber with enhanced moisture stability. *Angew. Chem. Int. Ed.* 53, 11232–11235
- Stoumpos, C.C. *et al.* (2016) Ruddlesden–Popper hybrid lead iodide perovskite 2D homologous semiconductors. *Chem. Mater.* 28, 2852–2867
- Niu, W. *et al.* (2014) Exfoliation of self-assembled 2D organic–inorganic perovskite semiconductors. *Appl. Phys. Lett.* 104, 171111
- Leng, K. *et al.* (2020) From bulk to molecularly thin hybrid perovskites. *Nat. Rev. Mater.* 5, 482–500
- He, X. *et al.* (2019) Oriented growth of ultrathin single crystals of 2D Ruddlesden–Popper hybrid lead iodide perovskites for high-performance photodetectors. *ACS Appl. Mater. Interfaces* 11, 15905–15912
- Stranks, S.D. and Plochocka, P. (2018) The influence of the Rashba effect. *Nat. Mater.* 17, 381–382
- Liu, X. *et al.* (2020) Circular photogalvanic spectroscopy of Rashba splitting in 2D hybrid organic–inorganic perovskite multiple quantum wells. *Nat. Commun.* 11, 323
- Kepenekian, M. *et al.* (2015) Rashba and Dresselhaus effects in hybrid organic–inorganic perovskites: from basics to devices. *ACS Nano* 9, 11557–11567

34. Jana, M.K. *et al.* (2020) Organic-to-inorganic structural chirality transfer in a 2D hybrid perovskite and impact on Rashba–Dresselhaus spin–orbit coupling. *Nat. Commun.* 11, 4699
35. Zheng, F. *et al.* (2015) Rashba spin–orbit coupling enhanced carrier lifetime in  $\text{CH}_3\text{NH}_3\text{PbI}_3$ . *Nano Lett.* 15, 7794–7800
36. Wang, T. *et al.* (2017) Indirect to direct bandgap transition in methylammonium lead halide perovskites. *Energy Environ. Sci.* 10, 509–515
37. Kim, M. *et al.* (2014) Switchable  $S = 1/2$  and  $J = 1/2$  Rashba bands in ferroelectric halide perovskites. *Proc. Natl. Acad. Sci. U. S. A.* 111, 6900
38. Bakulin, A.A. *et al.* (2015) Real-time observation of organic cation reorientation in methylammonium lead iodide perovskites. *J. Phys. Chem. Lett.* 6, 3663–3669
39. Mattoni, A. *et al.* (2015) Methylammonium rotational dynamics in lead halide perovskite by classical molecular dynamics: the role of temperature. *J. Phys. Chem. C* 119, 17421–17428
40. Ryu, H. *et al.* (2020) Static Rashba effect by surface reconstruction and photon recycling in the dynamic indirect gap of  $\text{APbBr}_3$  ( $A = \text{Cs}, \text{CH}_3\text{NH}_3$ ) single crystals. *J. Am. Chem. Soc.* 142, 21059–21067
41. Zhai, Y. *et al.* (2017) Giant Rashba splitting in 2D organic–inorganic halide perovskites measured by transient spectroscopies. *Sci. Adv.* 3, e1700704
42. Ichikawa, M. *et al.* (2002) Is  $\text{NaNO}_2$  a pure order–disorder type ferroelectric? *Solid State Commun.* 123, 135–139
43. Zhang, W. and Xiong, R.-G. (2012) Ferroelectric metal–organic frameworks. *Chem. Rev.* 112, 1163–1195
44. Ye, H.-Y. *et al.* (2018) Metal-free three-dimensional perovskite ferroelectrics. *Science* 361, 151
45. Horiuchi, S. and Tokura, Y. (2008) Organic ferroelectrics. *Nat. Mater.* 7, 357–366
46. Horiuchi, S. *et al.* (2010) Above-room-temperature ferroelectricity in a single-component molecular crystal. *Nature* 463, 789–792
47. Horiuchi, S. *et al.* (2008) Proton dynamics and room-temperature ferroelectricity in anilate salts with a proton sponge. *J. Am. Chem. Soc.* 130, 13382–13391
48. Horiuchi, S. *et al.* (2005) Ferroelectricity near room temperature in co-crystals of nonpolar organic molecules. *Nat. Mater.* 4, 163–166
49. Yang, C.-K. *et al.* (2019) The first 2D homochiral lead iodide perovskite ferroelectrics: [R- and S-1-(4-chlorophenyl)ethylammonium] $_2$ PbI $_4$ . *Adv. Mater.* 31, 1808088
50. Ji, C. *et al.* (2019) The first 2D hybrid perovskite ferroelectric showing broadband white-light emission with high color rendering index. *Adv. Funct. Mater.* 29, 1805038
51. Smith, M.D. and Karunadasa, H.I. (2018) White-light emission from layered halide perovskites. *Acc. Chem. Res.* 51, 619–627
52. Wang, S. *et al.* (2018) Highly efficient white-light emission in a polar two-dimensional hybrid perovskite. *Chem. Commun.* 54, 4053–4056
53. Wu, Z. *et al.* (2018) Alloying *n*-butylamine into  $\text{CsPbBr}_3$  to give a two-dimensional bilayered perovskite ferroelectric material. *Angew. Chem. Int. Ed.* 57, 8140–8143
54. Yang, Y. *et al.* (2021) Cooperative nature of ferroelectricity in two-dimensional hybrid organic–inorganic perovskites. *Nano Lett.* 21, 3170–3176
55. Zhang, H.-Y. *et al.* (2019) Toward the targeted design of molecular ferroelectrics: modifying molecular symmetries and homochirality. *Acc. Chem. Res.* 52, 1928–1938
56. Li, L. *et al.* (2019) Two-dimensional hybrid perovskite-type ferroelectric for highly polarization-sensitive shortwave photodetection. *J. Am. Chem. Soc.* 141, 2623–2629
57. Li, L. *et al.* (2018) Bilayered hybrid perovskite ferroelectric with giant two-photon absorption. *J. Am. Chem. Soc.* 140, 6806–6809
58. Li, L. *et al.* (2017) Tailored engineering of an unusual  $(\text{C}_4\text{H}_9\text{NH}_3)_2(\text{CH}_3\text{NH}_3)_2\text{Pb}_2\text{Br}_{10}$  two-dimensional multilayered perovskite ferroelectric for a high-performance photodetector. *Angew. Chem. Int. Ed.* 56, 12150–12154
59. Ye, H.-Y. *et al.* (2016) Bandgap engineering of lead-halide perovskite-type ferroelectrics. *Adv. Mater.* 28, 2579–2586
60. Liao, W.-Q. *et al.* (2015) A lead-halide perovskite molecular ferroelectric semiconductor. *Nat. Commun.* 6, 7338
61. Zhang, H.-Y. *et al.* (2020) Observation of vortex domains in a two-dimensional lead iodide perovskite ferroelectric. *J. Am. Chem. Soc.* 142, 4925–4931
62. Kim, Y.-H. *et al.* (2021) Chiral-induced spin selectivity enables a room-temperature spin light-emitting diode. *Science* 371, 1129
63. Lu, H. *et al.* (2020) Highly distorted chiral two-dimensional tin iodide perovskites for spin polarized charge transport. *J. Am. Chem. Soc.* 142, 13030–13040
64. Lu, H. *et al.* (2019) Spin-dependent charge transport through 2D chiral hybrid lead-iodide perovskites. *Sci. Adv.* 5, eaay0571
65. Li, P.-F. *et al.* (2016) Anomalous rotary polarization discovered in homochiral organic ferroelectrics. *Nat. Commun.* 7, 13635
66. Hua, X.-N. *et al.* (2018) A room-temperature hybrid lead iodide perovskite ferroelectric. *J. Am. Chem. Soc.* 140, 12296–12302
67. Zhang, Y. *et al.* (2015) Highly efficient red-light emission in an organic–inorganic hybrid ferroelectric: (pyrrolidinium)MnCl $_3$ . *J. Am. Chem. Soc.* 137, 4928–4931
68. Long, G. *et al.* (2020) Chiral-perovskite optoelectronics. *Nat. Rev. Mater.* 5, 423–439
69. Ai, Y. *et al.* (2019) Fluorine substitution induced high  $T_c$  of enantiomeric perovskite ferroelectrics: (R- and S)-3-(fluoropyrrolidinium)MnCl $_3$ . *J. Am. Chem. Soc.* 141, 4474–4479
70. Sha, T.-T. *et al.* (2019) Fluorinated 2D lead iodide perovskite ferroelectrics. *Adv. Mater.* 31, 1901843
71. Liu, H.-Y. *et al.* (2020) Molecular design principles for ferroelectrics: ferroelectrochemistry. *J. Am. Chem. Soc.* 142, 15205–15218
72. Yao, Y. *et al.* (2021) Exploring a fatigue-free layered hybrid perovskite ferroelectric for photovoltaic non-volatile memories. *Angew. Chem. Int. Ed.* 60, 10598–10602
73. Han, S. *et al.* (2021) Tailoring of a visible-light-absorbing biaxial ferroelectric towards broadband self-driven photodetection. *Nat. Commun.* 12, 284
74. Fong, D.D. *et al.* (2004) Ferroelectricity in ultrathin perovskite films. *Science* 304, 1650
75. Tybell, T. *et al.* (1999) Ferroelectricity in thin perovskite films. *Appl. Phys. Lett.* 75, 856–858
76. Fong, D.D. *et al.* (2006) Stabilization of monodomain polarization in ultrathin  $\text{PbTiO}_3$  films. *Phys. Rev. Lett.* 96, 127601
77. Junquera, J. and Ghosez, P. (2003) Critical thickness for ferroelectricity in perovskite ultrathin films. *Nature* 422, 506–509
78. Blancon, J.-C. *et al.* (2020) Semiconductor physics of organic–inorganic 2D halide perovskites. *Nat. Nanotechnol.* 15, 969–985
79. You, L. *et al.* (2018) In-plane ferroelectricity in thin flakes of van der Waals hybrid perovskite. *Adv. Mater.* 30, 1803249
80. Jia, F. *et al.* (2020) Persistent spin-texture and ferroelectric polarization in 2D hybrid perovskite benzylammonium lead-halide. *J. Phys. Chem. Lett.* 11, 5177–5183
81. Mao, L. *et al.* (2018) Hybrid Dion–Jacobson 2D lead iodide perovskites. *J. Am. Chem. Soc.* 140, 3775–3783
82. Ahmad, S. *et al.* (2019) Dion–Jacobson phase 2D layered perovskites for solar cells with ultrahigh stability. *Joule* 3, 794–806
83. Li, Y. *et al.* (2019) Bifunctional organic spacers for formamidinium-based hybrid Dion–Jacobson two-dimensional perovskite solar cells. *Nano Lett.* 19, 150–157
84. Park, I.-H. *et al.* (2019) Ferroelectricity and Rashba effect in a two-dimensional Dion–Jacobson hybrid organic–inorganic perovskite. *J. Am. Chem. Soc.* 141, 15972–15976
85. Wang, F. *et al.* (2020) Switchable Rashba anisotropy in layered hybrid organic–inorganic perovskite by hybrid improper ferroelectricity. *NPJ Comput. Mater.* 6, 183
86. Röhm, H. *et al.* (2017) Ferroelectric domains in methylammonium lead iodide perovskite thin-films. *Energy Environ. Sci.* 10, 950–955
87. Bi, F. *et al.* (2017) Enhanced photovoltaic properties induced by ferroelectric domain structures in organometallic halide perovskites. *J. Phys. Chem. C* 121, 11151–11158
88. Zhang, H.-Y. *et al.* (2020) Two-dimensional hybrid perovskite ferroelectric induced by perfluorinated substitution. *J. Am. Chem. Soc.* 142, 20208–20215

89. Isarov, M. *et al.* (2017) Rashba effect in a single colloidal CsPbBr<sub>3</sub> perovskite nanocrystal detected by magneto-optical measurements. *Nano Lett.* 17, 5020–5026
90. Becker, M.A. *et al.* (2018) Bright triplet excitons in caesium lead halide perovskites. *Nature* 553, 189–193
91. Yu, Z.-G. (2018) Estimation of the Rashba strength from second harmonic generation in 2D and 3D hybrid organic–inorganic perovskites. *J. Phys. Chem. C* 122, 29607–29612
92. Pham, M.T. *et al.* (2020) Origin of Rashba spin–orbit coupling in 2D and 3D lead iodide perovskites. *Sci. Rep.* 10, 4964
93. Chen, X. *et al.* (2018) Impact of layer thickness on the charge carrier and spin coherence lifetime in two-dimensional layered perovskite single crystals. *ACS Energy Lett.* 3, 2273–2279
94. Bernevig, B.A. *et al.* (2006) Exact SU(2) symmetry and persistent spin helix in a spin–orbit coupled system. *Phys. Rev. Lett.* 97, 236601
95. Kammermeier, M. *et al.* (2016) Control of spin helix symmetry in semiconductor quantum wells by crystal orientation. *Phys. Rev. Lett.* 117, 236801
96. Covaci, L. and Berciu, M. (2009) Polaron formation in the presence of Rashba spin–orbit coupling: implications for spintronics. *Phys. Rev. Lett.* 102, 186403
97. Edelstein, V.M. (1990) Spin polarization of conduction electrons induced by electric current in two-dimensional asymmetric electron systems. *Solid State Commun.* 73, 233–235
98. Sánchez, J.C.R. *et al.* (2013) Spin-to-charge conversion using Rashba coupling at the interface between non-magnetic materials. *Nat. Commun.* 4, 2944
99. Kepenekian, M. and Even, J. (2017) Rashba and Dresselhaus couplings in halide perovskites: accomplishments and opportunities for spintronics and spin–orbitronics. *J. Phys. Chem. Lett.* 8, 3362–3370
100. Wang, J. *et al.* (2019) Spin-optoelectronic devices based on hybrid organic–inorganic trihalide perovskites. *Nat. Commun.* 10, 129
101. Niesner, D. *et al.* (2018) Structural fluctuations cause spin-split states in tetragonal (CH<sub>3</sub>NH<sub>3</sub>)PbI<sub>3</sub> as evidenced by the circular photogalvanic effect. *Proc. Natl Acad. Sci. U. S. A.* 115, 9509
102. Niesner, D. *et al.* (2016) Giant Rashba splitting in CH<sub>3</sub>NH<sub>3</sub>PbBr<sub>3</sub> organic–inorganic perovskite. *Phys. Rev. Lett.* 117, 126401
103. Rivett, J.P.H. *et al.* (2018) Long-lived polarization memory in the electronic states of lead-halide perovskites from local structural dynamics. *Nat. Commun.* 9, 3531
104. Todd, S.B. *et al.* (2019) Detection of Rashba spin splitting in 2D organic–inorganic perovskite via precessional carrier spin relaxation. *APL Mater.* 7, 081116
105. Datta, S. and Das, B. (1990) Electronic analog of the electro-optic modulator. *Appl. Phys. Lett.* 56, 665–667
106. Di Sante, D. *et al.* (2013) Correction: Electric control of the giant Rashba effect in bulk GeTe. *Adv. Mater.* 25, 3625–3626
107. Leng, K. *et al.* (2020) Electron tunneling at the molecularly thin 2D perovskite and graphene van der Waals interface. *Nat. Commun.* 11, 5483
108. Tombros, N. *et al.* (2007) Electronic spin transport and spin precession in single graphene layers at room temperature. *Nature* 448, 571–574
109. Han, W. and Kawakami, R.K. (2011) Spin relaxation in single-layer and bilayer graphene. *Phys. Rev. Lett.* 107, 047207
110. Yamaguchi, T. *et al.* (2013) Electrical spin injection into graphene through monolayer hexagonal boron nitride. *Appl. Phys. Express* 6, 073001
111. Rashba, E.I. (2000) Theory of electrical spin injection: tunnel contacts as a solution of the conductivity mismatch problem. *Phys. Rev. B* 62, R16267–R16270
112. Wang, S. *et al.* (2019) An unprecedented biaxial trilayered hybrid perovskite ferroelectric with directionally tunable photovoltaic effects. *J. Am. Chem. Soc.* 141, 7693–7697
113. Huang, C.-R. *et al.* (2020) A multiaxial lead-free two-dimensional organic–inorganic perovskite ferroelectric. *Nat. Sci. Rev.* 8, nwa232
114. Zhang, Y. *et al.* (2020) Piezoelectric energy harvesting based on multiaxial ferroelectrics by precise molecular design. *Matter* 2, 697–710
115. Baudry, L. *et al.* (2017) Ferroelectric symmetry-protected multibit memory cell. *Sci. Rep.* 7, 42196
116. Sun, B. *et al.* (2020) Reversible thermochromism and strong ferromagnetism in two-dimensional hybrid perovskites. *Angew. Chem. Int. Ed.* 59, 203–208
117. Jungwirth, T. *et al.* (2012) Spin Hall effect devices. *Nat. Mater.* 11, 382–390
118. Manchon, A. *et al.* (2015) New perspectives for Rashba spin–orbit coupling. *Nat. Mater.* 14, 871–882
119. Choi, W.Y. *et al.* (2015) Electrical detection of coherent spin precession using the ballistic intrinsic spin Hall effect. *Nat. Nanotechnol.* 10, 666–670